Proceedings of ITC18, 2008

Practical Calculation of Nuclear Fusion Power for a Toroidal Plasma Device with Magnetic Confinement

P.R. Goncharov

St.Petersburg Polytechnical University, 195251, Russia

An algorithm has been developed and realized as a FORTRAN code to calculate the volume integral power of a magnetic confinement nuclear fusion reactor and the fusion rate function in a general case taking as input data the nuclei energy distributions, fusion cross-sections and the magnetic surface geometry. Two fast and simple analytic models of practical magnetic flux surface shapes have been introduced and the corresponding Jacobian determinants have been found. The developed method has been applied to obtain the radial profiles of the nuclear fusion reaction rate and the volume integral power for both Maxwellian and suprathermal D and T particle distributions. Gaussian kernel empirical probability density estimation has been proposed to reconstruct the ion energy probability density function from experimentally obtained random samples of escaping neutral atom energy. Neutral particle diagnostic database may serve as a basis for an experimentally confirmed calculation technique for reactor power and ignition criterion.

Keywords: fusion reactor power, nuclear fusion rate, ion distribution function, high energy particles, non-Maxwellian rate coefficients, plasma volume integration

1. Introduction

The power of a magnetic confinement fusion reactor P [W] and the fulfillment of the ignition criterion are quantitatively determined by the nuclear fusion reaction rate $\mathcal{R}_{\alpha\beta}$ [$m^{-3}s^{-1}$] integrated over the plasma volume using the known magnetic surface geometry:

$$P \propto \int \mathcal{R}_{\alpha\beta}(\mathbf{r}) d^3\mathbf{r} = \int \mathcal{R}_{\alpha\beta}(\rho,\vartheta,\varphi) R(\rho,\vartheta,\varphi) |J| \, d\rho d\vartheta d\varphi , \qquad (1)$$

where

$$J = \begin{vmatrix} \frac{\partial R}{\partial \rho} & \frac{\partial R}{\partial \vartheta} & 0 \\ \frac{\partial Z}{\partial \rho} & \frac{\partial Z}{\partial \vartheta} & 0 \\ 0 & 0 & 1 \end{vmatrix} \qquad (2)$$

is the Jacobian determinant for the transformation from cylindrical coordinates (R, Z, φ) to flux coordinates $(\rho, \vartheta, \varphi)$ with ρ, ϑ and φ designating the magnetic surface label, the poloidal angle and the toroidal angle respectively. Azimuthally symmetric magnetic surfaces are assumed in (2).

The rate of the nuclear fusion reaction between the species α and β,

$$\mathcal{R}_{\alpha\beta} = \frac{n_\alpha n_\beta}{1+\delta_{\alpha\beta}} \tilde{\mathcal{R}}_{\alpha\beta}, \qquad (3)$$

in turn, is proportional to the rate coefficient $\tilde{\mathcal{R}}_{\alpha\beta} = \langle \sigma(v) v \rangle$ averaged over the velocity distribution functions of the reacting species by integrating over the six-dimensional velocity space:

$$\tilde{\mathcal{R}}_{\alpha\beta} = \int \sigma(v) v f_\alpha(\mathbf{v}_\alpha) f_\beta(\mathbf{v}_\beta) d^3\mathbf{v}_\alpha d^3\mathbf{v}_\beta , \qquad (4)$$

where $v = |\mathbf{v}_\alpha - \mathbf{v}_\beta|$ is the relative velocity and $\delta_{\alpha\beta}$ is the Kronecker symbol reflecting the fact that when the reacting species are identical as in DD and TT reactions, and their density is n, the rate is proportional to $C_n^2 = \frac{1}{2} n(n-1) \approx \frac{n^2}{2}$.

The FORTRAN code for nuclear fusion rate and power calculation is based on (1) - (4) and nuclear cross-section approximations from [1-3]. Particle density profiles and the magnetic surface geometry are used as input data. Either analytic ion distribution functions based on theoretical models, or experimentally obtained ion distributions may be used for the calculations.

2. Analytic Models of Magnetic Surfaces

A rigorous treatment requires that Grad-Shafranov equation solutions are used. In order to increase the computation speed and simplify the code, two analytic models of magnetic surfaces have been used in the form of nested shifted D-shaped curves and nested shifted ellipses in the poloidal cross-section. The D-shaped last closed flux surface (LCFS) equation in cylindrical coordinates is

author's e-mail: goncharov@phtf.stu.neva.ru

$$Z^{\pm}_{LCFS}(R) = \pm\sqrt{(\kappa_1 + \kappa_2 R)} \times\sqrt{\sqrt{\kappa_3 R^2 + \kappa_4 R + \kappa_5} + \kappa_6 R + \kappa_7}\,, \qquad (5)$$

where $\kappa_1 = R_{out}/2\gamma$, $\kappa_2 = -1/2\gamma$, $\kappa_3 = 1-4\gamma$, $\kappa_4 = -2\left(\kappa_3 R_{out} + \delta(2\gamma-1)\right)$, $\kappa_5 = \kappa_3 R_{out}^2 + 2\delta \times(2\gamma-1)R_{out} + \delta^2$, $\kappa_6 = 1$ and $\kappa_7 = \delta - R_{out}$ are determined by three input parameters: outer plasma radius R_{out} [m], LCFS poloidal cross-section width δ [m] and dimensionless γ to control the LCFS poloidal cross-section width to height ratio. One more dimensional input parameter Δ [m] is to simulate the Shafranov shift. The magnetic axis position is then

$$R_0 = \frac{R_{in} + R_{out}}{2} + \Delta\,, \qquad (6)$$

where the inner plasma radius R_{in} [m] is calculated from the LCFS equation (5). The poloidal angle $\vartheta \in [0, 2\pi)$ is defined in the same way as the polar angle assuming $R = R_0$, $Z = 0$ to be the centre point and Z to be the polar axis.

As for the transformation between the cylindrical coordinates (R, Z, φ) and flux coordinates $(\rho, \vartheta, \varphi)$, the azimuthal (toroidal) angle $\varphi \in [0, 2\pi)$ preserves. For a given point (ρ, ϑ) in the poloidal plane the coordinate transformation to cylindrical (R, Z) is performed as follows. First,

$$\tilde{\vartheta} = \pi - (\pi - \vartheta)\, sign(\pi - \vartheta) \qquad (7)$$

is calculated, where $sign(y) = -1$ for $y < 0$ and $sign(y) = 1$ for $y \ge 0$. If $\tilde{\vartheta} = 0$, then $Z = 0$; $R = R_0 + \rho(R_{out} - R_0)$. If $\tilde{\vartheta} = \pi$, then $Z = 0$; $R = R_0 + \rho(R_{in} - R_0)$. If $\tilde{\vartheta} = \pi/2$, then $R = R_0$; $Z = \rho Z^{+}_{LCFS}(R_0)\, sign(\pi - \vartheta)$. Otherwise, the nonlinear equation

$$\frac{Z^{+}_{LCFS}(R_{LCFS})}{R_{LCFS} - R_0} - \tan\tilde{\vartheta} = 0 \qquad (8)$$

is resolved numerically with respect to R_{LCFS} sought within $[R_{in}, R_{out}]$. Then,

$$R = R_0 + \rho(R_{LCFS} - R_0)\,,$$
$$Z = \rho Z^{+}_{LCFS}(R_{LCFS})\, sign(\pi - \vartheta)\,. \qquad (9)$$

The ellipse-shaped LCFS equation in cylindrical coordinates is

$$Z^{\pm}_{LCFS}(R) = \pm\sqrt{\kappa_1 R^2 + \kappa_2 R + \kappa_3}\,, \qquad (10)$$

where $\kappa_1 = -b^2/a^2$, $\kappa_2 = 2b^2(R_{out} - a)/a^2$ and $\kappa_3 = b^2 - b^2(R_{out} - a)^2/a^2$ are determined by three

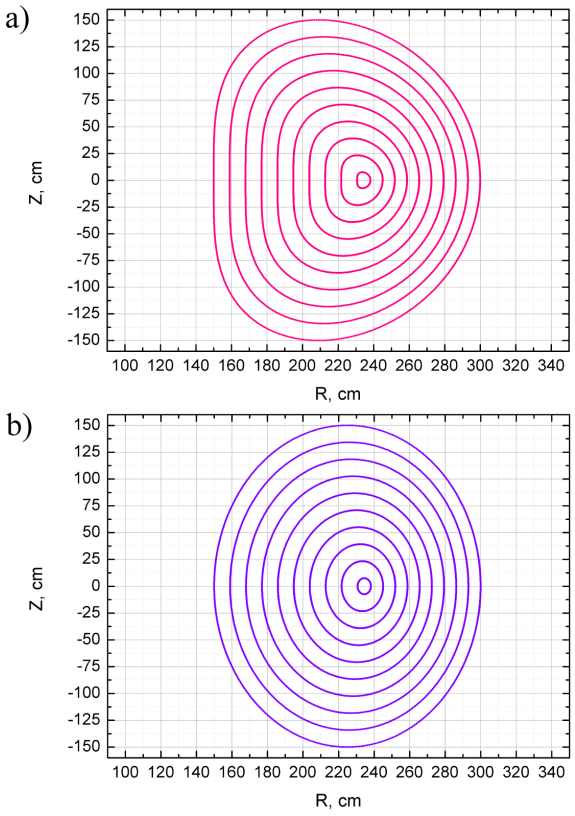

Fig. 1. a) D-shaped and b) ellipse-shaped isolines $\rho = const$ for R_{in} = 1.5 m, R_{out} = 3 m, Δ = 0.1 m.

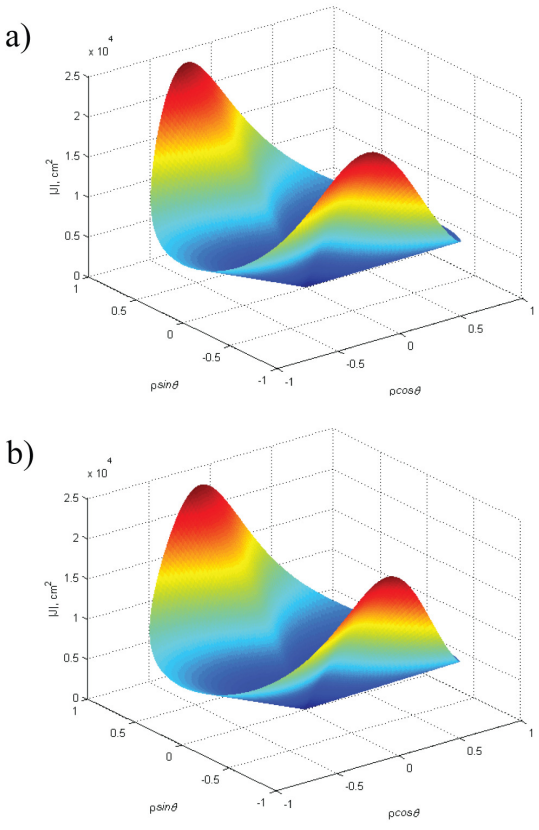

Fig. 2. Jacobian determinant for a) D-shaped and b) ellipse-shaped magnetic surface models.

dimensional input parameters: outer plasma radius R_{out} [m], major and minor ellipse semiaxes *a* [m] and *b* [m]. Again, one more dimensional input parameter Δ [m] is to simulate the Shafranov shift. The magnetic axis position is then

$$R_0 = R_{out} - a + \Delta . \qquad (11)$$

The coordinate transformation from (ρ, ϑ) to cylindrical (R, Z) is performed using formulas (8) and (9) analogously to the case of D-shaped curves substituting the proper function $Z^{+}_{LCFS}(R)$ given by (10) instead of (5).

Fig. 1 shows $\rho = const$ isolines obtained by using the coordinate transformation procedures for the two model magnetic surface shapes. The parameters are $\delta = 1.5$ m, γ = 0.326426 for Fig. 1 a); *a* = 0.75 m, *b* = 1.5 m for Fig. 1 b), R_{in} = 1.5 m, R_{out} = 3 m, Δ = 0.1 m for both.

Since R and Z are implicit functions of ρ and ϑ, central difference derivative formulas are used to calculate the elements of the Jacobian determinant (2). Left and right difference derivatives are used at the range $\rho \in [0,1]$, $\vartheta \in [0, 2\pi)$ extremities. The resulting $|J|$ shown in Fig. 2 enables one to calculate the volume integral (1) for either of the two magnetic surface types.

These fast simple analytic models or their combination may be used as a satisfactory practical approximation of a tokamak magnetohydrodynamic equilibrium whenever chord or volume integration, or mapping of plasma parameters as functions of magnetic surfaces to real space coordinates is required in physical and engineering tasks. For stellarator configurations more complicated full 3D models are needed.

3. Nuclear Fusion Rate Coefficients

3.1. Monoenergetic beam and Maxwellian target

For the monoenergetic and monodirectional distribution of species α interacting with a Maxwellian target β,

$$f_\alpha(\mathbf{v}_\alpha) = \delta(\mathbf{v}_\alpha - \mathbf{V}), \quad f_\beta(\mathbf{v}_\beta) = \left(\frac{m_\beta}{2\pi T}\right)^{3/2} e^{-\frac{m_\beta v_\beta^2}{2T}}, \qquad (12)$$

the rate coefficient (4) is reduced to

$$\tilde{\mathcal{R}}^{(BM)}_{\alpha\beta}\left(V, m_\beta/T\right) = \frac{1}{V}\left(\frac{2m_\beta}{\pi T}\right)^{1/2} e^{-\frac{m_\beta V^2}{2T}} \times \int_0^{+\infty} v^2 \sigma(v) \sinh\left(\frac{m_\beta v V}{T}\right) e^{-\frac{m_\beta v^2}{2T}} dv . \qquad (13)$$

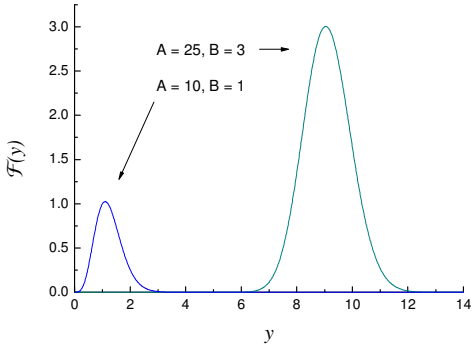

Fig. 3. Function $\mathcal{F}(y)$ in the integrand in (15).

Denoting the atomic velocity unit as $v_0 \approx 2.188\times10^8\ cm/s$ and introducing a dimensionless variable $y = v^2/v_0^2$ and dimensionless constants $A = \frac{m_\beta v_0^2}{2T}$ and $B = V/v_0$, consider a dimensionless function

$$\mathcal{F}(y) = \sqrt{y}\left(e^{2AB\sqrt{y} - Ay - AB^2} - e^{-2AB\sqrt{y} - Ay - AB^2}\right). \qquad (14)$$

Then,

$$\tilde{\mathcal{R}}^{(BM)}_{\alpha\beta}\left(V, m_\beta/T\right) = \frac{v_0}{2\sqrt{\pi}} \frac{\sqrt{A}}{B} \int_0^{+\infty} \sigma(y)\mathcal{F}(y) dy . \qquad (15)$$

To avoid arithmetic overflows, the constant e^{-AB^2} should not be taken outside the integral. $\mathcal{F}(y)$ is a nonnegative, slightly asymmetrically bell-shaped exponentially decaying function as shown in Fig. 3. The maximum position depends on the parameters. Qualitatively, function $\mathcal{F}(y)$ can very roughly be thought of as a Gaussian curve corresponding to the Maxwellian distribution of target particles, shifted along the abscissa axis by a value corresponding to the beam particle velocity. The exact maximum condition is expressed by a nonlinear equation

$$\tanh z = \frac{2AB^2 z}{z^2 - 2AB^2}, \qquad (16)$$

where $z = 2AB\sqrt{y}$. Equation (16) can be solved numerically, taking as an initial left-hand approximation to its root the positive root of the quadratic equation corresponding to the unit right hand side.

Assuming the cross-section $\sigma(y)$ to be a smoother function compared to $\mathcal{F}(y)$, the integral in

(15) can first be evaluated over a finite interval around the maximum of $\mathcal{F}(y)$. Then, at every subsequent step one should broaden the initially chosen arbitrary integration limits until the integral value becomes close enough to the one obtained at the previous step. Thus, the required relative precision may be achieved.

3.2. Isotropically distributed projectiles and Maxwellian target.

In the case when the velocity distribution of species α is expressed by an isotropic function $F(v_\alpha)$ and the distribution of species β is Maxwellian as in (12), the rate coefficient is calculated as

$$\tilde{\mathcal{R}}_{\alpha\beta}^{(FM)} = 4\pi \int_0^{+\infty} v_\alpha^2 F(v_\alpha) \tilde{\mathcal{R}}_{\alpha\beta}^{(BM)}\left(v_\alpha, m_\beta/T\right) dv_\alpha . \quad (17)$$

The technique to compute $\tilde{\mathcal{R}}_{\alpha\beta}^{(BM)}\left(v_\alpha, m_\beta/T\right)$ is described above. The practical realization of formula (17) depends on the specific function $F(v_\alpha)$. In particular, for suprathermal ion distributions occurring due to fast neutral beam injection heating the upper integration limit in practice appears to be finite. Another characteristic case of a bell-shaped exponentially decaying integrand implies that one should step-by-step broaden the integration range around the maximum position comparing the integral values until the required relative precision is achieved.

3.3. Isothermal Maxwellian case.

This is an important particular case of 3.2 above. For two Maxwellian species α and β at thermal equilibrium $T_\alpha = T_\beta = T$ the rate coefficient is

$$\tilde{\mathcal{R}}_{\alpha\beta}^{(MM)}\left(\mu_{\alpha\beta}/T\right) = \frac{2}{\sqrt{\pi}} v_0 \gamma^{3/2} \int_0^{+\infty} \sigma(y) f(y) dy , \quad (18)$$

where the dimensionless function $f(y) = ye^{-\gamma y}$, the dimensionless variable $y = v^2/v_0^2$ and the dimensionless constant $\gamma = \frac{\mu_{\alpha\beta} v_0^2}{2T}$. The value v_0, as above, denotes the atomic velocity unit and $\mu_{\alpha\beta} = m_\alpha m_\beta/(m_\alpha + m_\beta)$ is the reduced mass. The maximum of $f(y)$ is attained at $y = 1/\gamma$. Assuming the cross-section $\sigma(y)$ to be a smoother function compared to $f(y)$, the integral in (18) can first be evaluated over a finite interval around the maximum of $f(y)$. Then, at every subsequent step one should broaden the initially chosen arbitrary integration limits until the integral value becomes close enough to the one obtained at the previous step. Thus, the required relative precision may be achieved.

4. Fast Neutral Beam Injection-Induced Suprathermal Ion Distribution

In order to describe the neutral beam injection heating-induced fast ion distribution, one can use the classical nonstationary slowing down distribution function for a delta-like fast ion source

$$S\left(v_\alpha - v_{inj}\right) = \frac{S_0}{4\pi v_\alpha^2} \frac{e^{-\frac{\left(v_\alpha - v_{inj}\right)^2}{\epsilon^2}}}{\epsilon\sqrt{\pi}} \quad (19)$$

$$F\left(v_\alpha\right) = \frac{\mathrm{K}}{v_\alpha^3 + v_c^3}\left(erf\left(\frac{v^*\left(v_\alpha, t\right) - v_{inj}}{\epsilon}\right) - erf\left(\frac{v_\alpha - v_{inj}}{\epsilon}\right)\right), \quad (20)$$

where K is a normalization constant, the slowing down time

$$\tau_s = \frac{3 m_\alpha T_e^{3/2}}{4\sqrt{2\pi} n_e Z_\alpha^2 e^4 \Lambda m_e^{1/2}}, \quad (21)$$

cube of the critical velocity

$$v_c^3 = \frac{3\sqrt{2\pi} T_e^{3/2}}{2 m_\alpha m_e^{1/2}}, \quad (22)$$

Λ is the Coulomb logarithm, and, as shown in [4],

$$v^*\left(v_\alpha, t\right) = \left(\left(v_\alpha^3 + v_c^3\right) e^{3t/\tau_s} - v_c^3\right)^{1/3} . \quad (23)$$

The normalization constant K is determined by numerical integration. The ion velocity $v_\alpha = \sqrt{2E/m_\alpha}$, v_{inj} is the injection velocity corresponding to the injection energy E_{inj}, the values S_0 and ϵ in (19) determine the source rate and peak width, respectively, and t is the time since the commencement of the fast particle source action.

5. Experimentally Obtained Suprathermal Ion Distributions

Radial and angle dependence of the ion distribution function is studied experimentally by means of passive line-integral and also active localized charge exchange

neutral particle diagnostics [5, 6]. An extensive diagnostic database of this kind should enable one to predict the local ion distribution function evolution for a given plasma discharge regime in a certain device, for a specific heating method and time diagram.

Using the diagnostic data in the form of an array of energies (E_1, …, E_N) of escaped neutral particles measured along a certain observation direction, where N is the total number of particles collected during a certain time interval, one can construct an empirical probability density function

$$f^{(K)}(E) = \frac{1}{Nh}\sum_{j=1}^{N} K\left(\frac{E-E_j}{h}\right), \quad h>0 \qquad (24)$$

with Gaussian kernel function $K(z)=e^{-z^2/2}/\sqrt{2\pi}$. The optimal kernel bandwidth h selection algorithm and the ion distribution function reconstruction are discussed in [7].

Thus, a possibility exists to perform a correct experimentally confirmed calculation of the time evolution of the local fusion rate coefficient (4) and the fusion reactor power (1). Particular MHD equilibrium data can then be used rather than analytic approximations.

6. Calculation Examples

Assuming the radial density profiles to be

$$n_{e,D,T}(\rho)=\left(n_{e,D,T}(0)-n_{e,D,T}(1)\right)\left(1-\rho^a\right)^b+n_{e,D,T}(1) \qquad (25)$$

and radial temperature profiles

$$T_{e,D,T}(\rho)=\left(T_{e,D,T}(0)-T_{e,D,T}(1)\right)\left(1-\rho^q\right)^r+T_{e,D,T}(1), \qquad (26)$$

let us introduce an additive non-Maxwellian distortion of the form (20) to the deuterium distribution so that

$$f_D(\mathbf{v}_D)=A\left(\frac{m_D}{2\pi T}\right)^{3/2} e^{-\frac{m_D v_D^2}{2T}}+(1-A)F(v_D), \qquad (27)$$

where $A\le 1$. $A=1$ corresponds to the pure undistorted Maxwellian case. The rate coefficient for the interaction of deuterium particles distributed according to (27)

$$\tilde{\mathcal{R}}_{DD}=A^2\tilde{\mathcal{R}}_{DD}^{(MM)}\left(\mu_{DD}/T\right)+2A(1-A)\tilde{\mathcal{R}}_{DD}^{(FM)} +(1-A)^2\tilde{\mathcal{R}}_{DD}^{(FF)} \qquad (28)$$

is then calculated using (17) and (18). The last term in (28) accounts for the "tail-tail" particle interaction rate. It is considered negligible because the non-Maxwellian distortion is assumed to be small, *i.e.* $(1-A)^2 \ll 1$.

In the case when deuterium component distributed according to (27) interacts with Maxwellian tritons

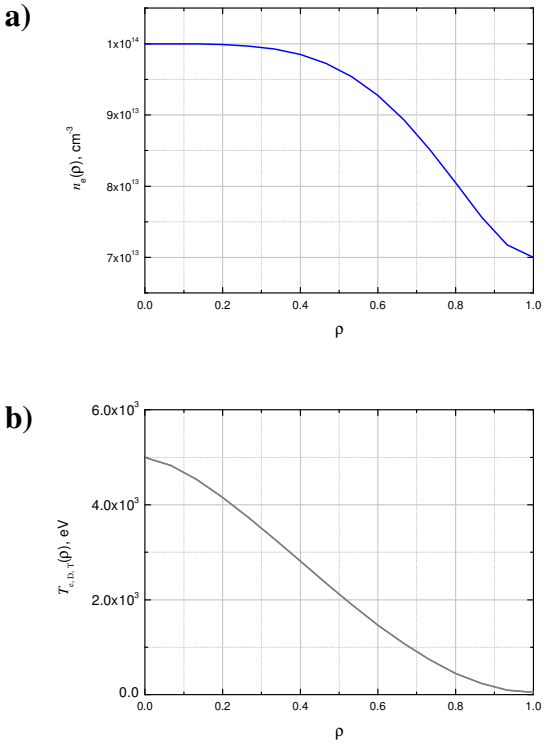

Fig. 4. a). Radial profile of deuterium and tritium density; b). Radial profile of deuterium and tritium temperature.

$$f_T(\mathbf{v}_T)=\left(\frac{m_T}{2\pi T}\right)^{3/2} e^{-\frac{m_T v_T^2}{2T}}, \qquad (29)$$

the rate coefficient is

$$\tilde{\mathcal{R}}_{DT}=A\tilde{\mathcal{R}}_{DT}^{(MM)}\left(\mu_{DT}/T\right)+(1-A)\tilde{\mathcal{R}}_{DT}^{(FM)}. \qquad (30)$$

The fusion rate radial profile and integral power calculation given below is for T(D,n)He^4 reaction. Fig. 4 a) shows the electron density profile with a = 4, b = 2, $n_e(0)=1.0\times10^{14}$ cm^{-3}, $n_e(1)=0.7\times10^{14}$ cm^{-3}. The nuclei densities are $n_D=n_T=n_e/2$. Fig. 4 b) shows the electron and ion temperature profile $T_e=T_D=T_T$ with q = 1.5, r = 2, $T_{e,D,T}(0)=5.0\times10^3$ eV, $T_{e,D,T}(1)=50$ eV.

Calculations have been performed for three variants of the deuteron velocity distribution function shown in Fig. 5, namely, for undistorted Maxwellian distribution and for the cases when there exists 2.5% or 5% population of suprathermal particles described by the classical slowing down model of beam particles with the injection energy E_{inj} = 150 keV. The non-locality, *i.e.*, the radial dependence

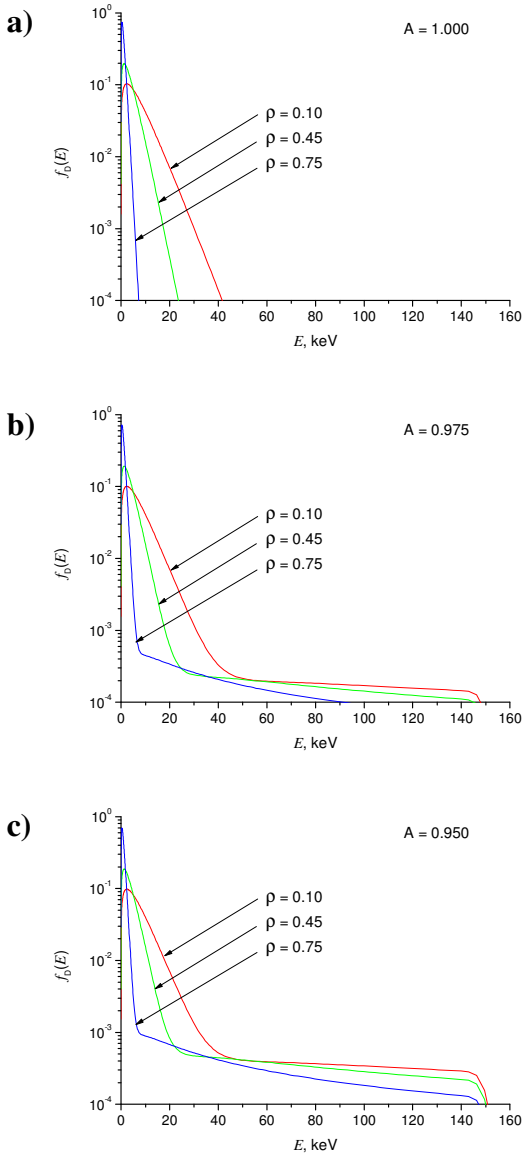

Fig. 5. Deuteron energy distribution function a) in the undistorted Maxwellian case for A = 1 and in the presence of suprathermal "tail" with b) A= 0.975 and c) A = 0.950.

of the ion distribution function in this model is due to the radial profiles of n_e and T_e, determining the slowing down time and the critical velocity values.

For each of the three variants of the distribution the radial profile of T(D,n)He^4 reaction rate has been calculated as well as the plasma volume integral power for two types of magnetic surfaces with D-shaped and elliptical poloidal cross-sections as shown in Fig. 1. Slight differences in the magnetic surface shape, as expected, have no significant direct "geometrical" influence on the power. Calculation results are shown in Fig. 6. In this example the presence of 5% suprathermal deuteron

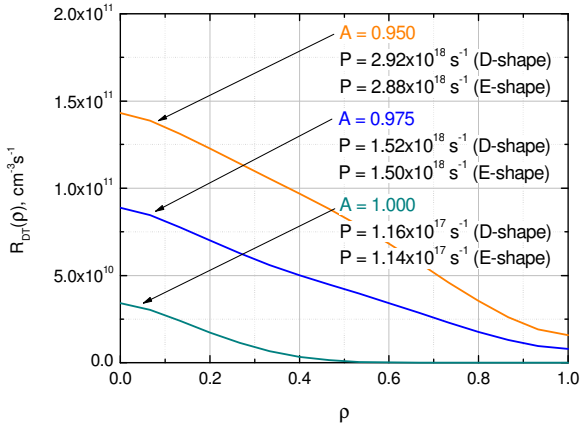

Fig. 6. Radial profiles of T(D,n)He^4 reaction rate for thermal tritons and three variants of deuteron energy distribution and the corresponding plasma volume integral power values for two types of magnetic surface geometry.

population leads to approximately 25 time increase in the fusion power compared to the pure Maxwellian case.

7. Summary

A general practical algorithm has been realized to calculate the nuclear fusion rate and power in a toroidal magnetic plasma confinement device. Volume integration is performed using analytical approximations of magnetic surfaces. A detailed description of velocity space integration technique for beam-Maxwellian, bi-Maxwellian and "isotropic function - Maxwellian" cases has been given. Fusion rate and power calculations can be done using either theoretical or experimentally obtained nuclei energy distribution functions.

A significant contribution to the nuclear fusion reaction rates comes from suprathermal ions from high-energy distribution tails. Therefore, the production and good confinement of fast ions play the essential role. Reliable experimental data and theoretical understanding of the formation of fast ion distribution tails are required.

The ion distribution function reflects the kinetic effects, the single particle confinement properties depending on the particular magnetic configuration, the finite β effects such as MHD induced fast ion losses, radial electric field effects, etc. As a method to investigate the ion component distribution function and its evolution due to the application of heating, measurements of kinetic energy distributions of neutral atoms escaping from the plasma may be used, which are often referred to as neutral particle analysis (NPA) diagnostics. Multidirectional passive measurements provide

information on the angular anisotropy, fast ion confinement, and distribution tail shapes. Line-integral energy-resolved neutral fluxes are obtained at different observation angles. Special mathematical techniques are required for the correct data analysis [5]. Another approach is to create a localized dense target for charge-exchange in the plasma. A diagnostic pellet ablation cloud can be used for this purpose (pellet charge exchange, or PCX method). Time-resolved measurements of the neutral flux from the cloud as it moves across the plasma column result in radially-resolved information on the fast particle energy distribution [6].

Smooth normalized probability density functions for the nuclei energies can then be calculated from NPA data using the method given in [7]. Thus, experimentally confirmed calculations of nuclear fusion rate and power are possible on the basis of diagnostic data.

References

[1] G.H. Miley, H. Towner, N. Ivich, Rept. COO-2218-17, University of Illinois (1974).

[2] B.H. Duane, Rept. BNWL-1685, Brookhaven National Laboratory (1972).

[3] H.-S. Bosch, G.M. Hale, Nucl. Fusion, **32**, 611 (1992).

[4] J.G. Cordey and M.J. Houghton, Nucl. Fusion, **13**, 215 (1973).

[5] P.R. Goncharov, T. Ozaki et al., Rev. Sci. Instrum., **79**, 10F311 (2008).

[6] P.R. Goncharov, T. Ozaki et al., Rev. Sci. Instrum., **79**, 10F312 (2008).

[7] P.R. Goncharov, T. Ozaki et al., Plasma and Fusion Research, **3**, S1083 (2008).